nature nanotechnology

LETTERS

PUBLISHED ONLINE: 11 MAY 2015 | DOI: 10.1038/NNANO.2015.78

Magnetoluminescence and valley polarized state of a two-dimensional electron gas in WS_2 monolayers

T. Scrace[1], Y. Tsai[1], B. Barman[1], L. Schweidenback[1], A. Petrou[1]*, G. Kioseoglou[2], I. Ozfidan[3,4], M. Korkusinski[3] and P. Hawrylak[3,4]*

Materials often exhibit fundamentally new phenomena in reduced dimensions that potentially lead to novel applications. This is true for single-layer, two-dimensional semiconductor crystals of transition-metal dichalcogenides, MX_2 (M = Mo, W and X = S, Se). They exhibit direct bandgaps with energies in the visible region at the two non-equivalent valleys in the Brillouin zone. This makes them suitable for optoelectronic applications that range from light-emitting diodes to light harvesting and light sensors[1–7], and to valleytronics[8–17]. Here, we report the results of a magnetoluminescence study of WS_2 single-layer crystals in which the strong spin–orbit interaction additionally locks the valley and spin degrees of freedom. The recombination of the negatively charged exciton in the presence of a two-dimensional electron gas (2DEG) is found to be circularly polarized at zero magnetic field despite being excited with unpolarized light, which indicates that the existence of a valley polarized 2DEG is caused by valley and spin locking and strong electron–electron interactions.

Tungsten-based dichalcogenides, such as WS_2, belong to the same family as MoS_2 and have many similar properties[15–17]; both compounds have the same structure and, in single layers, exhibit luminescence around 2 eV at the K points. The primary difference between MoS_2 and WS_2 is the strength of the spin–orbit splitting because of the different sizes of the transition-metal atoms. The photoluminescence (PL) efficiency of WS_2 is found to be much higher than that of MoS_2. In addition, the emission linewidth of the former is narrower, which makes WS_2 a better candidate for optoelectronic applications.

Despite extensive studies of these systems, there is very limited work on the effects of the application of an external magnetic field[12,13]. The purpose of the work in Sallen *et al.*[12] and Zeng *et al.*[13] was to investigate the Hanle effect by applying an in-plane magnetic field and demonstrate the intriguing result of the absence of such an effect. Very recently, Zhang *et al.*[7] reported circularly polarized electroluminescence from WSe_2 p–i–n junctions; the authors explain their results in terms of the breaking of the valley symmetry by an in-plane electric field[7]. In this work, we report spontaneous circularly polarized light emission from a single WS_2 layer excited by linearly polarized light at zero magnetic field. We attribute this effect to the existence of a spontaneously valley polarized 2DEG; this new state becomes possible in 2D materials because of valley and spin coupling along with strong electron–electron interactions.

The PL emission was found to contain two features: (1) the neutral exciton X^0 and (2) a broad feature at a lower energy related to the recombination of a valence hole in the presence of pockets of 2DEG owing to unintentional doping, which we will broadly classify as the negatively charged exciton, X^-, or Fermi edge singularity in the presence of a strong disorder[18–20]. The X^- feature discussed here is much broader than the corresponding feature in $MoSe_2$ reported by Ross *et al.*[11] because of the finite 2DEG density. Both X^- and X^0 features, show clear signatures in the reflectance spectrum. At zero magnetic field the X^- feature, related to the 2DEG, is circularly polarized light with a polarization of up to 18%, in direct contrast to the X^0 emission, which has no polarization. The spontaneous polarization of the emitted PL, excited with linearly polarized light, is attributed to the existence of a valley polarized 2DEG.

In Fig. 1a, we show the zero magnetic field PL spectrum (black line) and the first derivative (blue line) of the reflectance spectrum at $T = 5$ K. A picture of the sample used in our experiment is shown in Fig. 1b with a magnification of 100. Raman spectroscopy was used to determine which portions of the flake were single layers[15,21]. The PL spectrum was excited using linearly polarized light at 488 nm with an excitation power density of 2.04×10^2 W cm^{-2}. The strong PL emission below the free exciton energy is associated with the recombination of valence holes with a 2DEG present in different regions of the sample. In other words, the trion state has to be considered in the presence of a significant number of extra electrons distributed over different valley and spin states. In a material like GaAs, such a dense electron gas would lead to the breakdown of the trion and result in a Fermi-edge singularity. In transition-metal dichalcogenides, the binding energy of the exciton and the trion are much larger than those in materials such as GaAs; thus we expect the trion to be stabilized for much larger electron densities. The emission spectrum contains two features, labelled as X^0 and X^-. The identification of X^0 (at 2.053 eV) and X^- (at 2.014 eV) was made on the basis of previous work[22] as well as the fact that both X^0 and X^- have strong signatures in the reflectance spectrum[23].

One possible model that explains the coexistence of X^0 with the 2DEG feature is that the WS_2 crystal is inhomogeneous, possibly because of the inhomogeneous strain imposed by the substrate. This results in distinct regions: (1) regions with a different electron density from which we obtain the X^-–2DEG emission, and (2) regions with no electrons from which we obtain the X^0 emission, as extensively studied by a number of groups investigating gate-controlled 2DEG in semiconductor quantum wells[18–20]. The evolution of the PL with increasing temperature is shown in Fig. 1c for the $5\ \text{K} < T < 90\ \text{K}$ temperature range. It is clear from this

[1]University at Buffalo, SUNY, Buffalo, New York 14260, USA. [2]University of Crete, Heraklion GR-71003, Greece. [3]Quantum Theory Group, Emerging Technologies Division, National Research Council, Ottawa K1A 0R6, Ontario, Canada. [4]Department of Physics, University of Ottawa, Ottawa K1N 6N5, Ontario, Canada. *e-mail: petrou@buffalo.edu; pawel.hawrylak@uottawa.ca

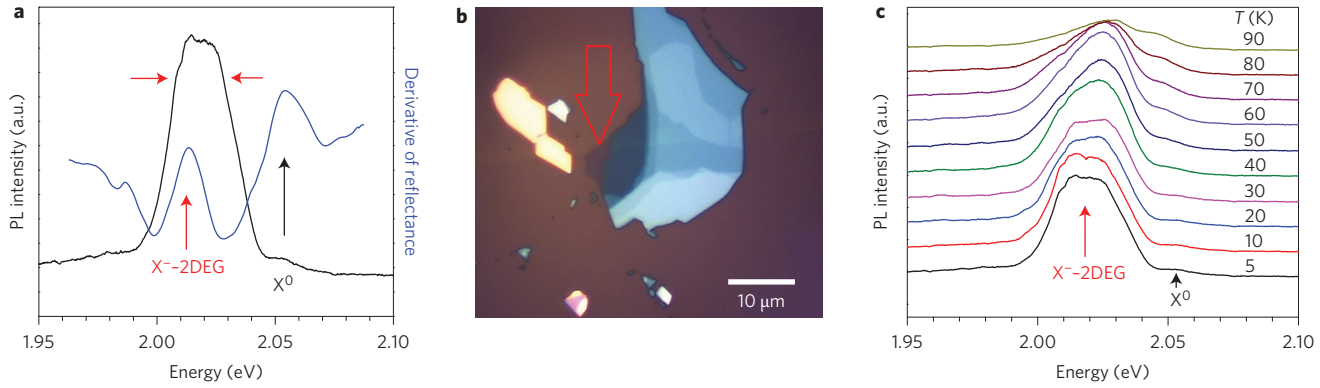

Figure 1 | PL spectra and optical image of monolayer WS_2. a, PL spectrum (not polarization resolved) for a 2.54 eV (488 nm) linearly polarized excitation at zero magnetic field and a temperature of 5 K. The spectrum consists of the neutral exciton X^0 and a broad feature at a lower energy attributed to the charged exciton emission in the presence of a 2DEG, X^-–2DEG. The blue curve is the first derivative of the reflectance spectrum, also taken at 5 K. **b**, Optical image of the WS_2 sample used in our experiments taken with a ×100 magnification. **c**, PL spectra (not polarization resolved) for a linearly polarized excitation at 2.54 eV for temperatures in the 5–90 K range.

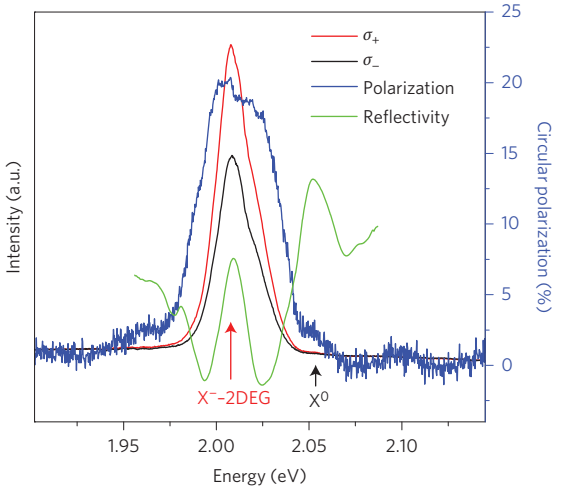

Figure 2 | Valley-spin polarization from a WS_2 monolayer at zero magnetic field and a temperature of 5 K. The PL was excited using linearly polarized light of photon energy 2.54 eV (488 nm). The red and black curves are the σ_+ and σ_- components of the PL spectra. A large (18%) spontaneous circular polarization appears for the X^-–2DEG recombination channel. The photon-energy dependence of the circular polarization is indicated by the blue curve (right *y*-axis); for comparison, we also superimpose the first derivative of the reflectance spectrum (green curve).

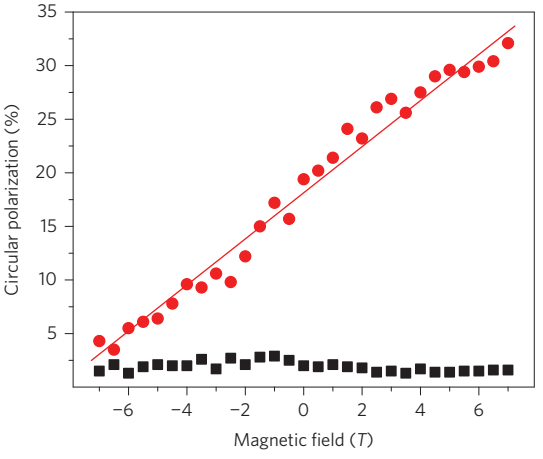

Figure 3 | Circular polarization as a function of magnetic field at a temperature of 5 K. The excitation was provided by linearly polarized light with a photon energy of 2.54 eV (488 nm). The PL was analysed for σ_+ and σ_- helicities and the polarization degree $P = (I_+ - I_-)/(I_+ + I_-)$ is plotted as a function of the applied magnetic field from –7 to +7 T. The red dots indicate the circular polarization of the X^-–2DEG emission and the black squares correspond to the polarization of the neutral exciton X^0 feature.

figure that, although the intensity of the X^0 PL feature relative to the intensity of the X^-–2DEG feature increases with increasing temperature, the X^- contribution persists because of the presence of the 2DEG and the large binding energy of the order of 30–35 meV[11].

The X^- PL feature is wide and contains contributions from other recombination channels. Typically, the PL linewidth is related to the number of occupied levels in the conduction band for a non-zero electron density with a finite Fermi energy as well as to contributions from other recombination channels. Indeed, at $T = 5$ K we have an impurity feature mixed in, as verified from the temperature dependence of the PL shown in Fig. 1c. When the sample temperature is increased, the impurity feature disappears. The high electron density could also result in an additional broadening that makes the width of the trion larger than that of the free exciton.

In Fig. 2 we plot the zero magnetic field reflectance derivative spectrum (green curve) and the σ_+ and σ_- PL components (red and black curves, respectively), excited using linearly polarized light at 488 nm at a power density of 2.04×10^2 W cm^{-2}. The PL circular polarization (blue curve) is given by the equation $P = (I_+ - I_-)/(I_+ + I_-)$, where I_+ and I_- are the intensities of the σ_+ and σ_- PL components, respectively. The two PL components exhibit a large difference in intensity, which results in a sizeable (18%) circular polarization at the energy of the X^-–2DEG PL feature. It is clear from Fig. 2 that the large zero-field circular polarization is related to the broad X^-–2DEG feature, whereas the circular polarization of the free exciton is only 2%. When we varied the excitation intensity F, we observed a modification of the emission-line shape consistent with a finite carrier density as well as a modest increase in the trion polarization at zero magnetic field. Typical values are $P = 15\%$ for $F = 1.02 \times 10^2$ W cm^{-2}, $P = 18\%$ for $F = 2.04 \times 10^2$ W cm^{-2} and $P = 23\%$ for $F = 2.04 \times 10^3$ W cm^{-2}. These results indicate that the observed zero-field circular polarization is an equilibrium property of the 2DEG and is not induced by the illumination of the sample.

In Fig. 3 we plot the circular polarization at $T = 5$ K of the X^-–2DEG and the X^0 features as a function of the magnetic field

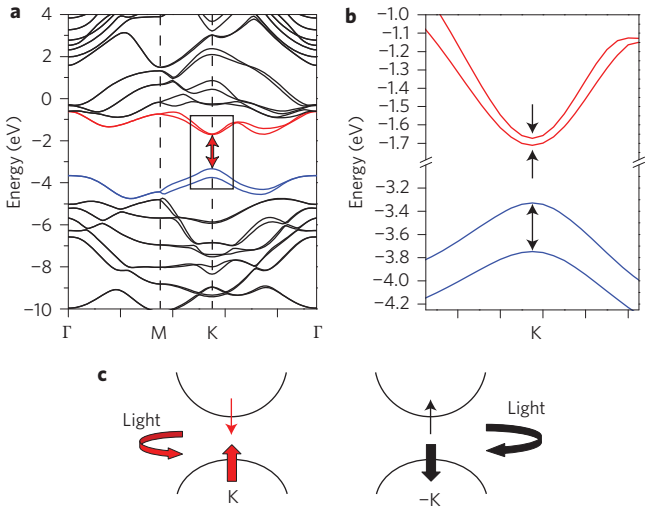

Figure 4 | Band structure and quantum numbers. a, Band structure of a single WS_2 layer computed using the ABINIT code; the diagram shows a direct gap at the K point of the Brillouin zone. **b**, The conduction and valence band state splitting in the vicinity of the K point caused by the spin–orbit interaction. **c**, Schematic illustration of the locking of the spin and valley quantum numbers.

applied along the normal to the sample plane. From Fig. 3 it is clear that the X^0 and the X^-–2DEG features differ in two aspects: (1) the X^-–2DEG feature has a non-zero polarization at $B = 0$ even though the exciting laser beam is linearly polarized and (2) the circular polarization of the exciton, X^0, is small and changes little with the magnetic field B. In contrast, the circular polarization of the X^-–2DEG feature increases with increasing B at a rate of 2% per tesla. We studied several single-layer WS_2 flakes. Each flake showed a positive non-zero circular polarization at $B = 0$ that strongly depends on B. An example of a circular polarization versus magnetic field plot from a different sample is shown in Supplementary Fig. 1.

The standard particle model of an equilibrium electron-spin polarization cannot produce a finite polarization at $B = 0$. The sample temperature does not have an appreciable effect on either the circular polarization at $B = 0$ (see Supplementary Fig. 2) or the slope dP/dB (see Supplementary Fig. 3). The circular polarization was studied as a function of the angle θ between the laser's linear polarization and the horizontal. A plot of circular polarization versus θ is shown in Supplementary Fig. 4. Finally, we compared the PL circular polarization for linearly and circularly polarized laser excitation. The results are given in Supplementary Fig. 5. Additional experiments showed a lack of dependence of the zero-field polarization on the way the B field was changed. As we discuss below, the experimental results can be understood assuming a spontaneous valley polarization (VP) of the 2DEG in WS_2 by locking of the spin and valley degrees of freedom.

Figure 4a shows results from an *ab initio* calculation of the band structure of a single neutral layer of WS_2 using the ABINIT code[24]. The results confirm that a single WS_2 layer is a 2D direct gap semiconductor with direct gaps at the six K points of the Brillouin zone. The local density approximation gap obtained here is 1.62 eV, in line with other work[11,21], but lower than the observed transition energy. This discrepancy (to be investigated) probably results from the self-energy and excitonic corrections as well as from strain and substrate effects.

Figure 4b shows the band structure of the K valley. The top of the valence band is split by 420 meV because of the spin–orbit coupling, and the analogous splitting of the conduction band is 38 meV. The corresponding hole mass is $m^* = 0.6m_0$ and the electron mass is $m^* = 0.5m_0$, where m_0 is a free electron mass. Figure 4c shows the spins of the conduction band electrons and valence band holes in the two non-equivalent valleys K and –K. Time-reversal symmetry requires that the two conduction band states (K,$s = -1/2$) and (–K, $s = +1/2$) be degenerate, with s denoting the electron spin. A similar, although more complicated, assignment can be made for the hole in the valence band. The locking of electron spin to the valley index caused by the large spin–orbit coupling uniquely relates the polarization of the emitted photon to the valley index, as shown in Fig. 4c. When a finite 2D electron density is present, electrons can occupy the two valleys (K,$s = -1/2$) and (–K,$s = +1/2$) with densities n_K and n_{-K}. For an ideal 2DEG, neglecting the formation of Landau levels, the total energy per particle (E_{tot}) is the sum of the kinetic, exchange, correlation and Zeeman energies[25,26]:

$$E_{tot}(r_s,\zeta) = \frac{1+\zeta^2}{r_s^2} - \frac{4\sqrt{2}}{3\pi}\frac{1}{r_s}\left[(1-\zeta)^{3/2} + (1+\zeta)^{3/2}\right] + E_c(r_s,\zeta) - \frac{g^*\mu_B B}{2}\zeta$$

where $n = (n_K + n_{-K})/2 = 1/\pi r_s^2$ is the total density, $\zeta = (n_K - n_{-K})/(n_K + n_{-K})$ is the valley-spin polarization and r_s is the interparticle distance. Energies and distances are measured in terms of the effective Rydberg (Ry) and the effective Bohr radius, respectively. The first term in E_{tot} is the contribution of kinetic energy, the second is the exchange energy, the third is the correlation energy (E_c) and the last term is the Zeeman energy. We see that VP costs kinetic energy but results in a gain of the exchange and Zeeman energy. The degeneracies of the energy spectrum are given by $E_{tot}(r_s,\zeta,B) = E_{tot}(r_s,-\zeta,-B)$. In Hartree–Fock the energy difference between the fully valley polarized state with $\zeta = 1$

$$E_{tot}(r_s,\zeta = 1) = \frac{2}{r_s^2} - \frac{16}{3\pi}\frac{1}{r_s} - \frac{g^*\mu_B B}{2}$$

and the unpolarized state with $\zeta = 0$

$$E_{tot}(r_s,\zeta = 0) = \frac{1}{r_s^2} - \frac{8\sqrt{2}}{3\pi}\frac{1}{r_s}$$

is given by

$$\Delta E = \frac{1}{r_s^2} - \frac{8(2-\sqrt{2})}{3\pi}\frac{1}{r_s} - \frac{g^*\mu B}{2}$$

At $B = 0$ the valley polarized states $\zeta = \pm 1$ are the ground states, with $\Delta E < 0$, for a range of densities δn_{VP} smaller than a critical density n^* with

$$\frac{1}{r_s} < \frac{8(2-\sqrt{2})}{3\pi}$$

or $r_s > 2$ ($r_s > 25.5$ when correlations are included (Attaccalite *et al.*[25] and Subasi and Tanatar[26])). The dependence of ΔE on $1/r_s$ is shown in black in the inset of Fig. 5. The coexistence of X^0 and the 2DEG-bound emission suggests that the sample is not homogeneous but consists of puddles, or quantum dots, with different densities. Assuming spontaneously broken symmetry selecting, for example, the $\zeta = +1$ state, puddles with

$$\frac{1}{r_s} < \frac{8(2-\sqrt{2})}{3\pi}$$

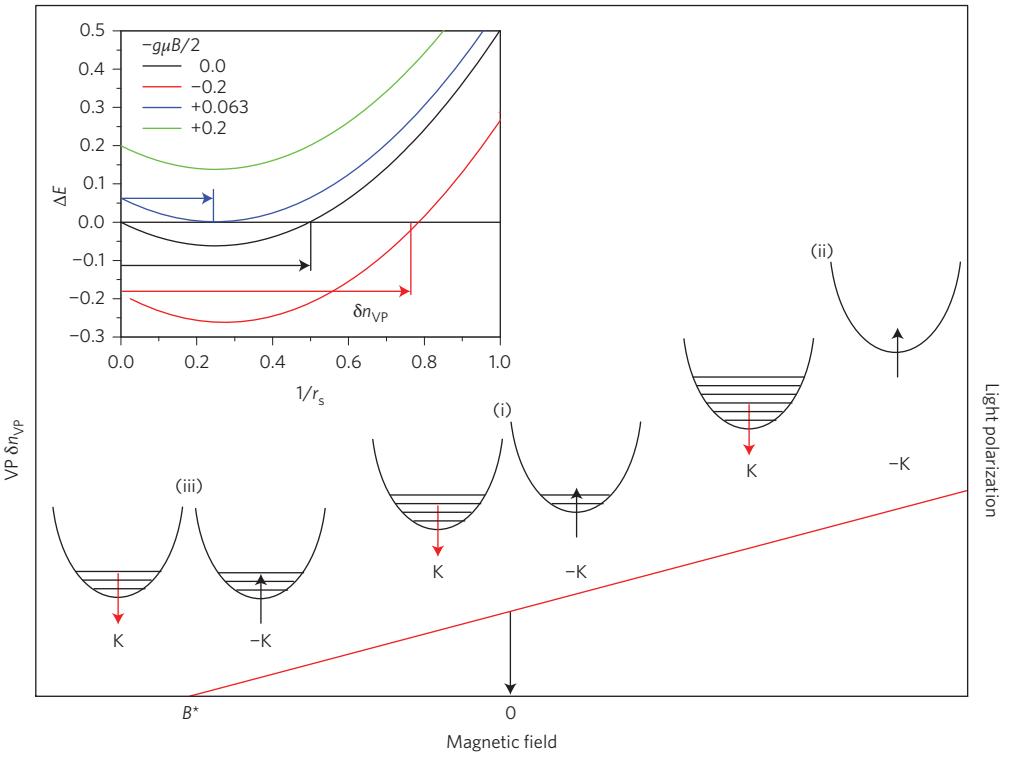

Figure 5 | Modelling of the dependence of the circular polarization on the magnetic field. The inset shows the energy difference per electron, ΔE (in effective Rydberg) between the valley polarized and the valley unpolarized states as a function of $1/r_s$ (r_s is expressed in terms of the effective Bohr radius). Negative values of ΔE correspond to the range of densities δn_{VP} for which the valley polarized state is the ground state. The main schematic illustrates the VP δn_{VP} as well as the circular polarization of the emitted light as a function of magnetic field. (i) $B = 0$, spontaneous VP; (ii) $B > 0$, increasing VP; (iii) $B < 0$, decreasing VP with B.

are valley polarized (the rest are not) which leads to partial valley and light polarization (for a detailed analysis of electron-spin polarization in quantum dots, see Korkusinski *et al.*[28]). Increasing the magnetic field B increases the range of densities δn_{VP} for which the ground state is the valley polarized state, as shown in red in the inset of Fig. 5. Reversing the direction of B applied to the $\zeta = +1$ state reduces the range of densities over which this valley polarized state is stable. At a critical value of negative B such that

$$g^*\mu|B^*| = 2\left[\frac{4(2-\sqrt{2})}{3\pi}\right]^2 \approx 0.125\,\mathrm{Ry}$$

(Fig. 5 inset, blue curve), the range of densities is reduced to a single value. For larger negative values of B (Fig. 5 inset, green curve), the valley unpolarized state is the lower energy state and the valley polarized state $\zeta = +1$ (Fig. 5 inset, green curve) can relax to the lowest energy state $\zeta = -1$ (Fig. 5 inset, red curve). The magnetic field dependence of the energy to flip the valley (and spin) of an electron in a valley polarized state depends on the density. For

$$\frac{1}{r_s} = \frac{4(2-\sqrt{2})}{3\pi}$$

the magnetic field dependence of $\Delta E(B)$ for the $\zeta = +1$ state can be written as

$$\Delta E(B) = -g^*\mu|B^*|/2 - g^*\mu B/2$$

where B^* is the effective exchange field. At $B = -|B^*|$ the external magnetic field compensates the exchange field B^* for this particular density. The effect of magnetic field on the range of densities δn_{VP} of the valley polarized ground state and degree of polarization of the emission is schematically illustrated in Fig. 5, where the symmetry of the population of the two valleys is spontaneously broken at $B = 0$, which results in a valley polarized state. As the valley population translates into the polarization of emitted light, the spontaneous VP leads to the spontaneous circular polarization of the emitted light, as shown experimentally in Fig. 3.

A similar calculation that accounts for the E_c was reported for an ideal 2DEG by, for example, Subasi and Tanatar[26], the effect of disorder was included in, for example, Narozhny *et al.*[27] and spin-polarized ground states in electronic puddles were discussed in Korkusinski *et al.*[28]. The existence of spin-polarized droplets in disordered 2DEG in semiconductor heterostructures was reported by Pepper and co-workers[29] and Pudalov and co-workers[30]. Although a detailed theory that accounts for a realistic electron-band structure, microscopic form of electron–electron interactions, including substrate, strain, density inhomogeneity and temperature, in WS_2 is needed, we present here strong evidence of a valley polarized electron gas in WS_2, with possible applications as a converter of unpolarized into polarized light. The valley polarized electron gas discussed above is not the only possible source of the observed spontaneous light polarization. Another possibility is that the polarization is caused by defects and grain boundaries. Further experiments are needed to distinguish between the different possibilities.

Methods

Methods and any associated references are available in the online version of the paper.

Received 11 July 2014; accepted 16 March 2015;
published online 11 May 2015

References

1. Mak, K. F., Lee, C., Hone, J., Shan, J. & Heinz, T. F. Atomically thin MoS_2: a new direct-gap semiconductor. *Phys. Rev. Lett.* **105,** 136805 (2010).
2. Splendiani, A. *et al.* Emerging photoluminescence in monolayer MoS_2. *Nano Lett.* **10,** 1271–1275 (2010).
3. Bernardi, M., Palummo, M. & Grossman, J. C. Extraordinary sunlight absorption and one nanometer thick photovoltaics using two-dimensional monolayer materials. *Nano Lett.* **13,** 3664–3670 (2013).
4. Korn, T., Heydrich, S., Hirmer, M., Schmutzler, J. & Schuller, C. Low-temperature photocarrier dynamics in monolayer MoS_2. *Appl. Phys. Lett.* **99,** 102109 (2011).
5. Perkins, F. K. *et al.* Chemical vapor sensing with mono layer MoS_2. *Nano Lett.* **13,** 668–673 (2013).
6. Wang, Q. H., Kalantar-Zadeh, K., Kis, A., Coleman, J. N. & Strano, M. S. Electronics and optoelectronics of two-dimensional transition metal dichalcogenides. *Nature Nanotech.* **7,** 699–712 (2012).
7. Zhang, Y. J., Oka, T., Suzuki, R., Ye, J. T. & Iwasa, Y. Electrically switchable chiral light-emitting transistor. *Science* **344,** 725–728 (2014).
8. Cao, T. *et al.* Valley-selective circular dichroism of monolayer molybdenum disulphide. *Nature Commun.* **3, 887** (2012).
9. Kioseoglou, G. *et al.* Valley polarization and intervalley scattering in monolayer MoS_2. *Appl. Phys. Lett.* **101,** 221907 (2012).
10. Mak, K. F., He, K. L., Shan, J. & Heinz, T. F. Control of valley polarization in monolayer MoS_2 by optical helicity. *Nature Nanotech.* **7,** 494–498 (2012).
11. Ross, J. S. *et al.* Electrical control of neutral and charged excitons in a monolayer semiconductor. *Nature Commun.* **4,** 1 (2013).
12. Sallen, G. *et al.* Robust optical emission polarization in MoS_2 monolayers through selective valley excitation. *Phys. Rev. B* **86,** 081301 (2012).
13. Zeng, H. L., Dai, J. F., Yao, W., Xiao, D. & Cui, X. D. Valley polarization in MoS_2 monolayers by optical pumping. *Nature Nanotech.* **7,** 490–493 (2012).
14. Mak, K. F., McGill, K. L., Park, J. & McEuen, P. L. The valley Hall effect in MoS_2 transistors. *Science* **344,** 1489–1492 (2014).
15. Gutierrez, H. R. *et al.* Extraordinary room-temperature photoluminescence in triangular WS_2 monolayers. *Nano Lett.* **13,** 3447–3454 (2013).
16. Jones, A. M. *et al.* Spin-layer locking effects in optical orientation of exciton spin in bilayer WSe_2. *Nature Phys.* **10,** 130–134 (2014).
17. Zhao, W. J. *et al.* Evolution of electronic structure in atomically thin sheets of WS_2 and WSe_2. *ACS Nano* **7,** 791–797 (2013).
18. Skolnick, M. S. *et al.* Observation of a many-body edge singularity in quantum-well luminescence spectra. *Phys. Rev. Lett.* **58,** 2130–2133 (1987).
19. Hawrylak, P. Optical-properties of a 2-dimensional electron-gas – evolution of spectra from excitons to Fermi-edge singularities. *Phys. Rev. B* **44,** 3821–3828 (1991).
20. Yusa, G., Shtrikman, H. & Bar-Joseph, I. Charged excitons in the fractional quantum Hall regime. *Phys. Rev. Lett.* **87,** 216402 (2001).
21. Berkdemir, A. *et al.* Identification of individual and few layers of WS_2 using Raman spectroscopy. *Sci. Rep.* **3,** 1–8 (2013).
22. Mitioglu, A. A. *et al.* Optical manipulation of the exciton charge state in single-layer tungsten disulfide. *Phys. Rev. B* **88,** 245403 (2013).
23. Kioseoglou, G. *et al.* Photoluminescence and reflectance studies of negatively charged excitons in $GaAs/Al_{0.3}Ga_{0.7}As$ quantum-well structures. *Phys. Rev. B* **61,** 4780–4785 (2000).
24. Kadantsev, E. S. & Hawrylak, P. Electronic structure of a single MoS_2 monolayer. *Solid State Commun.* **152,** 909–913 (2012).
25. Attaccalite, C., Moroni, S., Gori-Giorgi, P. & Bachelet, G. B. Correlation energy and spin polarization in the 2D electron gas. *Phys. Rev. Lett.* **88,** 256601 (2002).
26. Subasi, A. L. & Tanatar, B. Effects of a parallel magnetic field on the ground-state magnetic properties of a two-dimensional electron gas. *Phys. Rev. B* **78,** 155304 (2008).
27. Narozhny, B. N., Aleiner, I. L. & Larkin, A. I. Magnetic fluctuations in two-dimensional metals close to the Stoner instability. *Phys. Rev. B* **62,** 14898–14911 (2000).
28. Korkusinski, M., Sheng, W. & Hawrylak, P. Designing quantum systems in self-assembled quantum dots. *Phys. Status Solidi B* **238,** 246–249 (2003).
29. Ghosh, A., Ford, C. J. B., Pepper, M., Beere, H. E. & Ritchie, D. A. Possible evidence of a spontaneous spin polarization in mesoscopic two-dimensional electron systems. *Phys. Rev. Lett.* **92,** 116601 (2004).
30. Teneh, N., Kuntsevich, A. Y., Pudalov, V. M. & Reznikov, M. Spin-droplet state of an interacting 2D electron system. *Phys. Rev. Lett.* **109,** 226403 (2012).

Acknowledgements

The authors thank S. Banerjee and his group at SUNY Buffalo for technical support. Work at SUNY Buffalo has been supported by the Office of Naval Research. I.O., M.K. and P.H. acknowledge support of National Research Council Quantum Photonic Sensing and Security program and of the Natural Sciences and Engineering Research Council. G.K. acknowledges support by the Greek General Secretariat for Research and Technology project ERC02-EXEL (contract No. 6260).

Author contributions

T.S., Y.T., B.B., L.S., A.P. and G.K. designed and performed the experimental measurements, and I.O., M.K. and P.H. provided the theoretical analysis. A.P., G.K., M.K. and P.H. wrote the manuscript.

Additional information

Supplementary information is available in the online version of the paper. Reprints and permissions information is available online at www.nature.com/reprints. Correspondence and requests for materials should be addressed to A.P. and P.H.

Competing financial interests

The authors declare no competing financial interests.

Methods

The samples used in our experiments were purchased from 2D Semiconductors and consist of flakes of WS_2. The flakes were deposited on a silicon substrate topped with a 90 nm layer of SiO_2. The WS_2 flakes were exfoliated from bulk WS_2 crystals. Raman spectroscopy was used to determine which portions of the flakes were single layers. The samples were placed on the cold finger of a continuous-flow optical cryostat operated in the 5–300 K temperature range. The cryostat was mounted on a three-axis translator with a spatial resolution of 10 μm in the x and y directions and 5 μm along the z direction. The cryostat tail was positioned inside the room-temperature bore of a 7 T superconducting magnet.

The photoluminescence was excited using the 488 nm or 514.5 nm lines from an argon-ion laser. A collimated white-light beam was used for the reflectivity work. The incident light was focused on the sample using a microscope objective with a working distance of 34 mm. The combination of the objective and the other lenses of the optical set-up gave an overall magnification of ×50.

The same objective collected the emitted luminescence (reflected light in the reflectivity experiments) from the sample in a Faraday geometry and the light was focused onto the entrance slit of a single monochromator equipped with a cooled CCD (charge-coupled device) detector array. The spectrometer was equipped with a long focal length microscope/CCD camera combination. A flip mirror allowed us to direct the light that passes through the entrance slit of the spectrometer to either the microscope or the CCD detector. The light from the sample was analysed in its σ_+ and σ_- circularly polarized components by a combination of a liquid-crystal quarter-wave plate and a linear polarizer placed before the entrance slit of the spectrometer.